Modification of the saturation model: Dokshitzer-Gribov-Lipatov-Altarelli-Parisi evolution

J. Bartels
II. Institut für Theoretische Physik, Universität Hamburg, Luruper Chaussee 149, D-22761 Hamburg, Germany

K. Golec-Biernat
II. Institut für Theoretische Physik, Universität Hamburg, Luruper Chaussee 149, D-22761 Hamburg, Germany and H. Niewodniczański Institute of Nuclear Physics, Kraków, Poland

H. Kowalski
Deutsches Electronen Synchrotron DESY, Hamburg, Germany

(Received 10 May 2002; published 28 June 2002)

We propose to modify the saturation model of Golec-Biernat and Wüsthoff by including Dokshitzer-Gribov-Lipatov-Altarelli-Parisi evolution. We find considerable improvement for the total deep inelastic cross section, in particular in the large Q^2 region. The successful description of deep inelastic scattering diffraction is preserved.

DOI: 10.1103/PhysRevD.66.014001 PACS number(s): 13.60.Hb, 12.38.Bx

The saturation model [1–3] has provided a successful description of DESY *ep* collider HERA deep inelastic scattering (DIS) data, in particular for the transition from the perturbative region to the nonperturbative photoproduction region. This includes both the total $\gamma^* p$ cross section and the DIS diffractive cross section. Whereas the formulas are particularly appealing through their simplicity, they also have an attractive theoretical background, namely, the idea of saturation. Despite its success, the model suffers from shortcomings which should be cured. In particular, the model does not include logarithmic scaling violations; i.e., at larger values of Q^2 it does not exactly match with QCD evolution [Dokshitzer-Gribov-Lipatov-Altarelli-Parisi (DGLAP)]. This becomes clearly visible in the energy dependence of $\sigma_{tot}^{\gamma^* p}$ in the region $Q^2 > 20$ GeV^2 where the model predictions are below the data. One expects that QCD evolution should enhance the cross section in this region.

It is the purpose of this paper to propose a modification of the saturation model. We attempt to preserve the success of the model in the low-Q^2 and in the transition regions, while incorporating DGLAP evolution in the large-Q^2 domain. Since the energy dependence in the large-Q^2 region is mainly due to the behavior of the dipole cross section at small dipole sizes r, our changes will affect mostly the small-r region. At the same time, particular attention will be given to DIS diffraction for which the saturation model correctly describes the energy dependence. Since the inclusive diffractive cross section mostly depends upon the large-r behavior of the dipole cross section, we attempt to leave the dipole cross section unchanged in this region. A recent attempt [4] along the same lines indicates that, in fact, diffraction provides a highly nontrivial restriction on possible modifications of the saturation model.

I. THE MODEL

Before we describe the modifications of the saturation model, we briefly review the main features of its original formulation. Within the dipole formulation of the $\gamma^* p$ scattering,

$$\sigma_{T,L}^{\gamma^* p}(x,Q^2) = \int d^2 r \int dz \, \psi_{T,L}^*(Q,r,z)\, \hat{\sigma}(x,r) \times \psi_{T,L}(Q,r,z), \tag{1}$$

where T,L denotes the virtual photon polarization, the dipole cross section was proposed to have the form

$$\hat{\sigma}(x,r) = \sigma_0 \left\{ 1 - \exp\left(-\frac{r^2}{4R_0^2(x)} \right) \right\}, \tag{2}$$

where $R_0(x)$ is the saturation scale which decreases when $x \to 0$,

$$R_0^2(x) = \frac{1}{\mathrm{GeV}^2} \left(\frac{x}{x_0} \right)^{\lambda}. \tag{3}$$

In order to be able to study the formal photoproduction limit, the Bjorken variable $x = x_B$ was modified to be

$$x = x_B \left(1 + \frac{4m_q^2}{Q^2} \right) = \frac{Q^2 + 4m_q^2}{W^2}, \tag{4}$$

where m_q is an effective quark mass, and W^2 denotes the $\gamma^* p$ center-of-mass energy squared. The parameters of the model, $\sigma_0 = 23$ mb, $\lambda = 0.29$ and $x_0 = 3 \times 10^{-4}$ (for the assumed quark mass $m_q = 140$ MeV) were found from a fit to small-x data [1]. For alternative forms of the dipole cross section parametrization see [5].

As it is well known [6], in the small-r region the dipole cross section is related to the gluon density

$$\hat{\sigma}(x,r) \simeq \frac{\pi^2}{3} r^2 \alpha_s x g(x,\mu^2), \tag{5}$$

where the scale μ^2 for small r behaves as C/r^2. Equation (5) is valid in the double logarithmic approximation in which the constant C is not determined. In the saturation model, Eq. (2), we find for small $r \ll 2R_0(x)$

$$\hat{\sigma}(x,r) \simeq \frac{\sigma_0 r^2}{4\,R_0^2(x)}, \tag{6}$$

i.e., the gluon density is modeled as

$$xg(x,\mu^2) = \frac{3}{4\pi^2\alpha_s}\frac{\sigma_0}{R_0^2(x)}. \tag{7}$$

For fixed α_s this gluon density is clearly scale independent, which contradicts the QCD DGLAP evolution. Thus, in order to correctly take into account the scale dependence as given by the DGLAP evolution equations we have to modify the small-r behavior of the dipole cross section by incorporating the properly evolved gluon density. At the same time, we wish to preserve the idea of saturation, which reflects unitarity, and to keep unaltered the large-r behavior of the dipole cross section which determines the diffractive cross section.

Therefore, we propose the following modification of the model (2):

$$\hat{\sigma}(x,r) = \sigma_0\left\{1 - \exp\left(-\frac{\pi^2 r^2 \alpha_s(\mu^2) x g(x,\mu^2)}{3\,\sigma_0}\right)\right\}, \tag{8}$$

where the scale μ^2 is assumed to have the form

$$\mu^2 = \frac{C}{r^2} + \mu_0^2. \tag{9}$$

The parameters C and μ_0^2 will be determined from a fit to DIS data. In a first approximation, $g(x,\mu^2)$ is evolved with the leading order DGLAP evolution equation for the gluon density. In the spirit of the small-x limit, we neglect quarks in the evolution equations. We assume the following gluon density at the initial scale $Q_0^2 = 1$ GeV^2:

$$xg(x,Q_0^2) = A_g x^{-\lambda_g}(1-x)^{5.6}, \tag{10}$$

where A_g and λ_g are parameters to be determined from a fit to data. The exponent 5.6, determining the large-x behavior, is motivated by one of the versions of the Martin-Roberts-Stirling-Thorne (MRST) parametrization [7] of the gluon density.

For small r, the exponential in Eq. (8) can be expanded in powers of its argument, and the relation (5), with the running $\alpha_s = \alpha_s(\mu^2)$, is found. In contrast to the original dipole cross section, the rise in $1/x$ now has become r dependent. When inserting $\hat{\sigma}$ into Eq. (1) and convoluting with the photon wave function, the integrand peaks near $r \sim 2/Q$ for large Q^2, and the argument of the gluon density turns into $\mu^2 \approx Q^2$. Consequently, with increasing Q^2, DGLAP evolution will strengthen the rise in $1/x$, whereas in the original saturation model the power of $1/x$ had been constant. For sufficiently large r, the scale μ^2 is frozen at the value μ_0^2. This prevents the effective scale of the gluon density from becoming unreasonably small. The saturation value of the dipole cross section is $\hat{\sigma}(x,r) \approx \sigma_0$, as in the original model (2). The transition from the small to the large r region depends on x, but in detail it will be different from the original model. This will be discussed in detail in the section presenting numerical results.

II. MOMENTUM SPACE FORMULATION

Although in this paper we will restrict ourselves to the total (and later on to the diffractive) cross section, it is instructive to rephrase these features in momentum space. In a future step, we intend to study the effects of saturation in more exclusive final states, and the translation of our dipole cross section into momentum space may serve as a first step into this direction. For this purpose let us start with the k_T-fatorization formula [8] for the $\gamma^* p$ cross section, e.g. for the transversely polarized photon [9],

$$\sigma_T^{\gamma^* p} = \frac{\alpha_{em}}{\pi}\sum_f e_f^2 \int_0^1 dz[z^2 + (1-z)^2] \times \int d^2\mathbf{k} \int \frac{d^2\mathbf{l}}{l^4}\alpha_s f(x,l^2) \times \left\{\frac{\mathbf{k}}{\mathbf{k}^2+\bar{Q}^2} - \frac{\mathbf{k}+\mathbf{l}}{(\mathbf{k}+\mathbf{l})^2+\bar{Q}^2}\right\}^2, \tag{11}$$

where $f(x,l^2)$ is the gluon amplitude describing an interaction of the $q\bar{q}$ pair with the proton, $\mathbf{l}$ is the transverse momentum of the gluon coupled to the quark pair and $\bar{Q}^2 = z(1-z)Q^2$. Using the relation

$$\frac{\mathbf{k}}{\mathbf{k}^2+\bar{Q}^2} = i\bar{Q}\int \frac{d^2\mathbf{r}}{2\pi} e^{i\mathbf{k}\cdot\mathbf{r}}\frac{\mathbf{r}}{r}K_1(\bar{Q}r), \tag{12}$$

the following formula is found:

$$\sigma_T^{\gamma^* p} = \frac{3\alpha_{em}}{2\pi^2}\sum_f e_f^2 \int_0^1 dz[z^2+(1-z)^2]\bar{Q}^2 \times \int d^2\mathbf{r}\int d^2\mathbf{r}'\frac{\mathbf{r}\cdot\mathbf{r}'}{rr'}K_1(\bar{Q}r)K_1(\bar{Q}r') \times \int \frac{d^2\mathbf{k}}{(2\pi)^2}e^{i\mathbf{k}\cdot(\mathbf{r}-\mathbf{r}')}D(\mathbf{r},\mathbf{r}'), \tag{13}$$

where

$$D(\mathbf{r},\mathbf{r}') = \frac{2\pi}{3}\int \frac{d^2\mathbf{l}}{l^4}\alpha_s f(x,l^2)(1-e^{i\mathbf{l}\cdot\mathbf{r}})(1-e^{-i\mathbf{l}\cdot\mathbf{r}'}). \tag{14}$$

If the argument of the strong coupling α_s and the variable x in the gluon amplitude in $D(\mathbf{r},\mathbf{r}')$ do not depend on the

quark transverse momenta $\mathbf{k}$, the integration over $\mathbf{k}$ in Eq. (13) gives the delta function $\delta^2(\mathbf{r}-\mathbf{r}')$ which reflects the conservation of a dipole transverse size vector $\mathbf{r}$ during the collision. In this case the dipole formula (1) is obtained with the following identification of the dipole cross section:

$$\hat{\sigma}(x,\mathbf{r})=\frac{2\pi}{3}\int\frac{d^2\mathbf{l}}{l^4}\alpha_s f(x,l^2)(1-e^{i\mathbf{l}\cdot\mathbf{r}})(1-e^{-i\mathbf{l}\cdot\mathbf{r}}). \tag{15}$$

Going beyond the leading $\log(1/x)$ approximation in which Eq. (11) was derived, e.g. by taking into account the exact gluon kinematics [10] or considering a quark virtuality $\mathbf{k}^2+\overline{Q}^2$ as an argument of the running coupling α_s, we find that $\mathbf{r}$ is no longer conserved during the scattering process, and the simple relation (15) ceases to exist. As a result, the k_T-factorization formula (11) can no longer be written in the form (1), and the simple dipole picture fails. We want to avoid this situation, thus we assume that the argument of α_s is given by the gluon momentum $\mathbf{l}^2$ and $x=x_{Bj}$. Since the integration in Eq. (15) includes also small momenta, the modeling of the infrared behavior of α_s cannot be avoided. However, we will hide this fact by analyzing the combined quantity $\alpha_s f(x,l^2)$.

From the requirement that in the double logarithmic limit (DLL) formula (11) should be consistent with the DLL of the DGLAP formalism one can derive a relation between the gluon amplitude $f(x,l^2)$ and the conventional gluon distribution $xg(x,Q^2)$. Starting from Eq. (11), using the relation $F_T=Q^2/(4\pi^2\alpha_{em})\sigma_T^{\gamma^* p}$ and imposing the strong ordering condition: $\mathbf{l}^2\ll\mathbf{k}^2\ll Q^2$, one arrives at

$$\frac{\partial F_T(x,Q^2)}{\partial\log Q^2}=\frac{1}{3\pi}\sum_f e_f^2\int^{Q^2}\frac{d^2\mathbf{l}}{\pi l^2}\alpha_s f(x,l^2). \tag{16}$$

By comparison with an analogous formula obtained in the DLL of the DGLAP evolution equations, one finds the following relation at large Q^2:

$$\alpha_s(Q^2)xg(x,Q^2)=\int^{Q^2}\frac{d^2\mathbf{l}}{\pi l^2}\alpha_s f(x,l^2). \tag{17}$$

In the model (8) we go beyond the k_T-factorization formula (11) where $f(x,l^2)$ represent a two-gluon amplitude. In the region of small l^2, the relation (17) between $f(x,l^2)$ and the gluon density no longer holds, and $f(x,l^2)$ is defined through relation (15), where for the left-hand side (lhs) we use our model (8). In general, provided the dipole cross section has a finite limit: $\lim_{r\to\infty}\hat{\sigma}(x,r)=\hat{\sigma}_\infty(x)$, Eq. (15) can be inverted with the help of the following relation:

$$\begin{aligned}\frac{\alpha_s f(x,l^2)}{l^4}&=\frac{3}{4\pi}\int\frac{d^2\mathbf{r}}{(2\pi)^2}\exp\{i\mathbf{l}\cdot\mathbf{r}\}\\&\quad\times\{\hat{\sigma}_\infty(x)-\hat{\sigma}(x,r)\}\\&=\frac{3}{8\pi^2}\int_0^\infty dr\,r\,J_0(lr)\{\hat{\sigma}_\infty(x)-\hat{\sigma}(x,r)\}.\end{aligned} \tag{18}$$

In the original dipole model we find [2]

$$\alpha_s f(x,l^2)=\frac{3\sigma_0}{4\pi^2}R_0^2(x)l^4\exp\{-R_0^2(x)l^2\}. \tag{19}$$

For the modified dipole cross section, this inversion has to be done numerically. DGLAP evolution will affect mainly the large-l behavior while at small l our modification should be less severe. The most interesting question to be addressed below concerns the transition region: to what extent does our modification affect the region of moderate momenta, i.e. could one ''see'' saturation in diffractive final states?

III. NUMERICAL RESULTS

Let us now turn to numerical results. We performed global fits to the DIS data with $x<0.01$ in the range of Q^2 between 0.1 and 500 GeV^2. For H1 and ZEUS HERA experiments the new 1996–1997 data sets were used [11–13]. In addition to the HERA data also the data of the E665 experiment [14] were used. The statistical and systematic errors were added in quadrature. The number of degrees of freedom, N_{df}, was around 330.

The new data sets are considerably more precise (with much smaller statistical and systematic errors) than the ones used in the original analysis [1]. As a preparatory step, we applied the original model (2), using the parameter values of the original fit, to the new data and obtained a rather high value of $\chi^2/N_{df}\sim 3$ (for the old data, the corresponding value was $\chi^2/N_{df}=1.18$). Next, we allowed the new data to determine their own values of the parameters of the original model, σ_0, λ and x_0 in Eq. (2). This led to an improvement of the fit, $\chi^2/N_{df}\sim 2.2$. Nevertheless, this relatively poor agreement indicates that the original model is doing not so well with the new data, especially for large values of Q^2. As a first step for the improvement, we modify the dipole cross section at small values of r by including QCD DGLAP evolution, as given in Eq. (8).

In the modified saturation model, there are five parameters to be determined: σ_0, C, μ_0^2, A_g and λ_g from Eqs. (8), (9), (10). We use the leading order DGLAP evolution equation for the gluon density, and we put $\Lambda_{QCD}=200$ MeV in α_s and set the number of active flavors $N_f=3$. Thus, although the evolution equation for the gluon is decoupled from the quarks, their presence is encoded in the assumed value of N_f.

We performed first the fit leaving all five parameters free and assumed the value of the light quark mass $m_q=140$ MeV, as in the original formulation [1]. A good quality fit was obtained with $\chi^2/N_{df}=1.05$. The found value of

TABLE I. The parameters of the fits to the ZEUS, H1 and E665 data with $x<0.01$ (333 points). The H1 data were rescaled by a factor of 1.05. The numbers in bold are fixed during the fits.

	m_q(MeV)	σ_0 (mb)	A_g	λ_g	C	μ_0^2	χ^2/N_{df}
Fit 1	**140**	**23.0**	1.20	0.28	0.26	0.52	1.17
Fit 2	0	23.8	13.71	−0.41	11.10	**1.00**	0.97

the dipole cross section $\sigma_0=27.4$ mb, however, was higher than the saturation model value, $\sigma_0=23$ mb. Also, the corresponding value of the photoproduction cross section ($\sigma^{\gamma p}=204$ mb) was significantly higher than the measured value $174\pm1(st)\pm13(sys)$ mb at $W=209$ GeV [15]. Thus we decided to decrease σ_0 and fixed it to the saturation model value 23 mb. This value is also advantageous for the description of the inclusive DIS diffractive cross section which is more sensitive to large dipole sizes, i.e., to the saturation region, than the total γ^*p cross section [2]. The resulting parameters in such fit are presented in Table I (**Fit 1**). The description is slightly worse than that described above, but both the photoproduction cross section ($\sigma^{\gamma p}=189$ mb) and the diffractive cross section are properly described. This is because we modified only the small dipole size part of the dipole cross section (2), without affecting the saturation part. The found gluon density gives 39% of the total proton momentum carried by gluons resolved at the initial scale $Q_0^2=1$ GeV^2.

The results of Fit 1 are compared to the data on F_2 in Fig. 1 for $Q^2<1$ GeV^2 and in Fig. 2 for large Q^2 points. In all presented plots, the solid lines refer to the results obtained with the DGLAP improved model (8) and the dashed lines correspond to the saturation model (2) with the original parameters from [1]. We see that the DGLAP evolution significantly improves agreement with the data at large Q^2 while at small Q^2 the results are practically the same. This effect is summarized in Fig. 3 where the effective slopes $\lambda(Q^2)$, obtained from the parametrization of F_2 at small x: $F_2\sim x^{-\lambda(Q^2)}$, are plotted. Thus, the DGLAP modification of the dipole cross section for small r is crucial for much better agreement with the data. The same effective slopes characterize the energy dependence of the γ^*p cross section: $\sigma^{\gamma^*p}\sim(W^2)^{\lambda(Q^2)}$. The change from a soft dependence at small Q^2 to a hard one for large Q^2 is shown in Fig. 4. In Fig. 5 we show another aspect of the transition of F_2 to low Q^2 values, namely the emergence of the behavior: $F_2\sim Q^2$ approached in the limit $Q^2\to0$ and $y=W^2/s$ fixed. The class of the saturation models described here nicely reproduces this behavior; see recent Ref. [16] for more details on this transition.

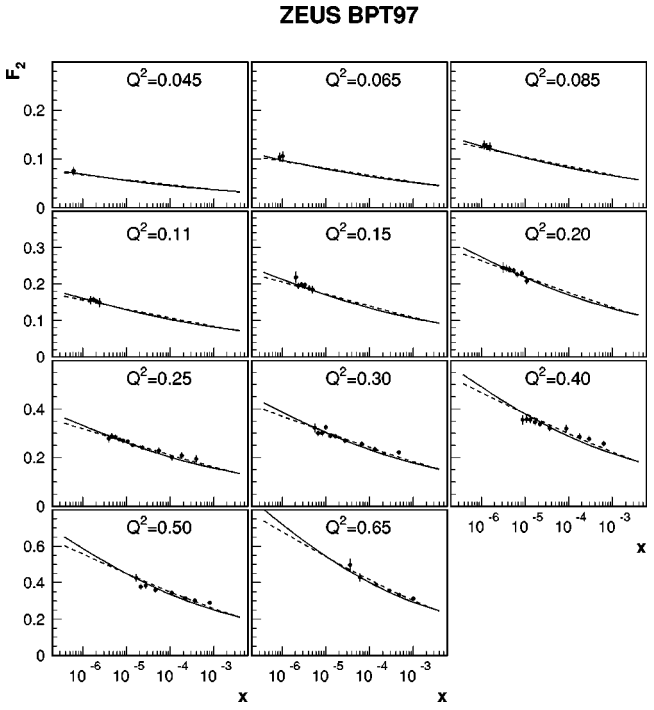

FIG. 1. F_2 as a function of x for fixed low Q^2 values. A comparison with the low Q^2 data from ZEUS. The solid lines indicate the model with the DGLAP evolution (8) (Fit 1) and the dotted lines indicate the saturation model (2).

In the second step of our investigations we relax our requirement of staying in the low-Q^2 region as close as possible to the original model. In particular, we allow the quarks in the $q\bar{q}$ dipole to become massless. Thus we set $m_q=0$ in the wave function $\Psi_{T,L}$ and in the kinematic relation (4). In the original model, the quark mass was introduced as an effective parameter for modeling the large-r behavior of the photon wave function. The non-zero quark mass allows us to study the photoproduction limit of our model after the modification (4) of the Bjorken-x in the dipole cross section; therefore, setting this parameter to zero eliminates this possibility. It allows, however, for a better description of the current data. We also fix the minimal value μ_0^2 of the scale μ^2 in Eq. (8) to 1 GeV^2 in the fits in order to avoid negative gluon density below the input scale $Q_0^2=1$ GeV^2 for the gluon evolution.[1] Since the parameters σ_0 and λ_g are strongly correlated, we have performed a systematic search of the best χ^2 on the grid of fixed (σ_0, λ_g). In each case, the remaining parameters, A_g and c, were fitted. In this way we found two local minima for χ^2, shown in Fig. 6, for a positive value of λ_g in Eq. (10) leading to strongly rising gluon density, and for a negative value of λ_g, corresponding to the valence-like initial gluon. The latter scenario gives a considerable better description (with $\chi^2/N_{df}=0.97$) than the first one (with $\chi^2/N_{df}=1.13$). In the final analysis, after a quan-

[1]The valence-like gluon density preferred in the massless fit, as described in the text, becomes negative below the input scale due to backward evolution. In this case the dipole cross section (8) does not saturate at large r.

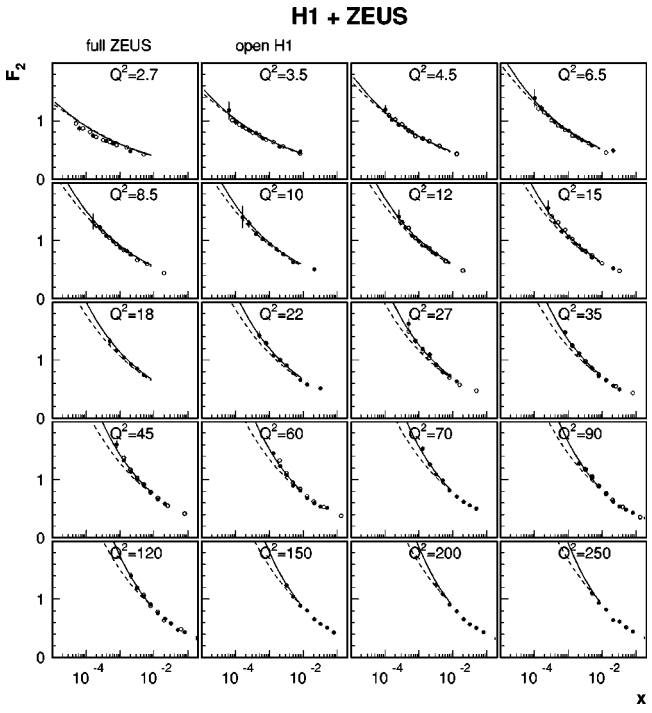

FIG. 2. H1 and ZEUS data on F_2 as a function of x for fixed values of $Q^2>1$ GeV^2 and the saturatiom model curves. The solid lines indicate the model with the DGLAP evolution (8) (Fit 1) andthe dotted lines indicate the saturation model (2).

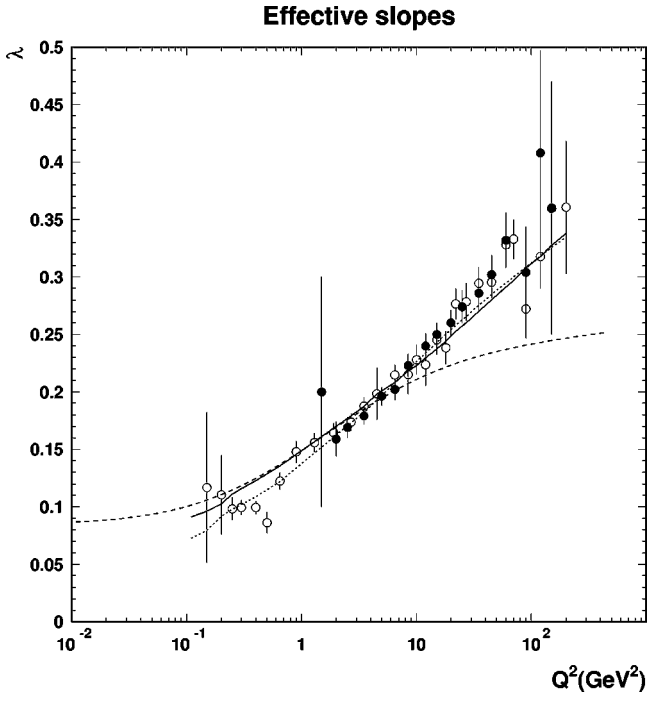

FIG. 3. The effective slope $\lambda(Q^2)$ from the parametrization $F_2 \sim x^{-\lambda(Q^2)}$ as a function of Q^2. The model with the DGLAP evolution (8): the solid line (Fit 1) and the dotted line (Fit 2). The saturation model (2): the dashed line. The ZEUS analysis: the open circles. The H1 data [20]: the full circles.

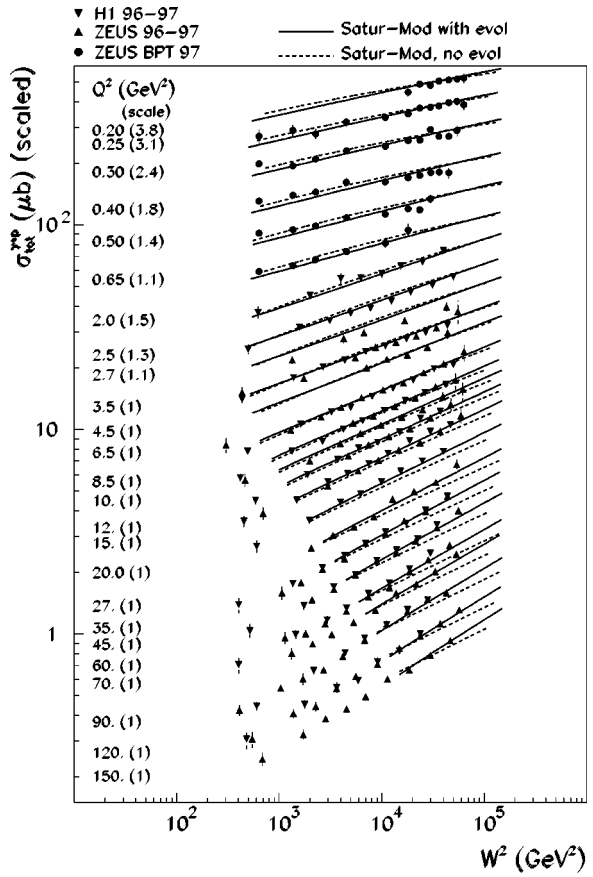

FIG. 4. The $\gamma^* p$ cross section as a function of energy W^2 at various Q^2. The solid lines: the model with the DGLAP evolution (8) (Fit 1). The dotted line: the saturation model (2), shown for $x<0.01$.

titative estimation of the position of the best fit in the parameter space using the grid method, we allow σ_0 and λ_g to be fitted together with A_g and c. The values of these parameters for the best fit are given in Table I (**Fit 2**). The corresponding value of the gluon momentum at the input scale equals 84%. The effective slope $\lambda(Q^2)$ from the Fit 2 parametrization is shown as the dotted line in Fig. 3. As expected, slight differences between the two fit scenarios only appear for small values of Q^2, below 1 GeV^2.

It is interesting to compare the results of the Fit 1 and Fit 2 since they lead to a different picture of the dynamics of the $\gamma^* p$ interaction. In Fit 1 the initial gluon density, $xg(x,Q_0^2)$, quickly rises with $1/x$, whereas in Fit 2 it even decreases with rising $1/x$. Therefore, in Fit 1 the rise of the cross section with the energy is mainly due to the intrinsic properties of the initial gluon density, with only slight corrections being due to the evolution effects at high Q^2 values, and considerable damping effects resulting from saturation at low Q^2. In Fit 2 the evolution effects are very strong (note the value of the parameter C, which is much higher then in Fit 1). The small-x rise of the cross section is due solely to the DGLAP evolution effects with some corrections coming from saturation.

Further insight into the physical picture lying behind the fits can be gained by a closer look at the r dependence of the

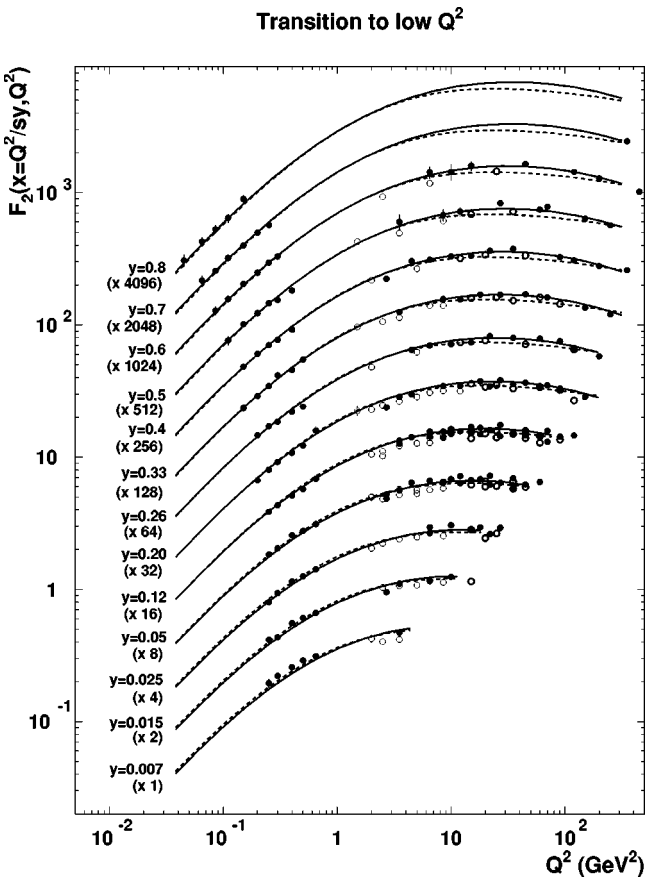

FIG. 5. $F_2(x,Q^2)$ as a function of Q^2 for fixed $y=Q^2/(sx)$. The solid lines: the model with DGLAP evolution (8) (Fit 1). The dashed lines: the saturation model (2). The curves are plotted for $x<0.01$. Full circles: ZEUS data. Open circles: H1 data.

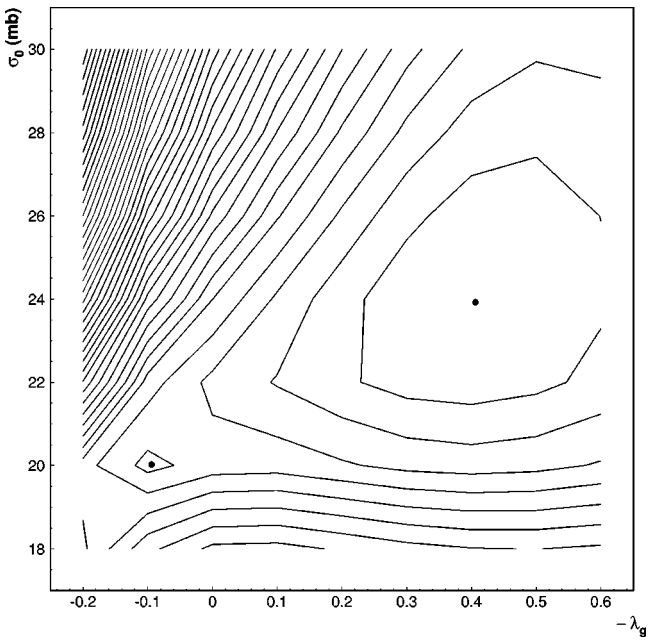

FIG. 6. The lines of constant values of χ^2 in the space of $(\sigma_0,-\lambda_g)$ in the massless case, $m_q=0$. The two local minima are indicated by the black dots. The one for $-\lambda_g\simeq 0.4$ corresponds to Fit 2.

dipole cross section $\hat{\sigma}(x,r)$, and a momentum dependence of the related gluon amplitude, $f(x,l^2)$. In the first row of Fig. 7 we show the dipole cross section for the two fits. As we have already discussed, for Fit 1 the DGLAP modification (solid lines) affects mostly the region of moderately small r (<1 GeV^{-1}). In Fit 2 both the small and large r regions are affected. In particular, the structure close to the saturation region is different from that in the saturation model (2) (dashed lines). The differences between the models are particular visible if we turn to momentum space and compute the gluon amplitude $\alpha_s f(x,l^2)$ for different values of x, using relation (18). The results are shown in the second row of Fig. 7, where the full lines denote the gluon amplitude from the DGLAP improved model and the dashed lines correspond to the saturation model (2). The small r region of the dipole cross section corresponds to the large l^2 region in the gluon amplitude. The dipole cross section from Fit 1 is translated into a gluon amplitude with a double-bump structure. Notice that the second bump results from the DGLAP modification of the small-r part of the dipole cross section. In Fit 2, however, the second bump disappears and the gluon amplitude is similar but significantly broader than the one corresponding to the saturation model. Although in Fig. 7 the various gluon amplitudes are clearly distinct, after convolution with the impact factors and turning to the $\gamma^* p$ cross sections, these differences are becoming much less visible. It is natural to expect that some of these differences should become visible in more exclusive final states. As a first example, one might think of DIS diffraction. The inclusive diffractive process, however, is sensitive to the region of small l^2 or large r and, therefore, has only limited value in distinguishing between the two fit solutions. On the other hand, other physics processes like jet, charm and bottom production should be more sensitive to the behavior of the unintegrated gluon density at large gluon momenta l^2.

Looking at Fig. 7 notice that starting from certain values of l^2, the gluon amplitudes become negative. In order to understand this let us differentiate the relation (17) with respect to the large scale μ^2,

$$\alpha_s f(x,\mu^2)\simeq\frac{\partial}{\partial\ln\mu^2}\{\alpha_s(\mu^2)xg(x,\mu^2)\}$$
$$=\alpha_s(\mu^2)\left\{\frac{\partial xg(x,\mu^2)}{\partial\ln\mu^2}-\frac{xg(x,\mu^2)}{\ln(\mu^2/\Lambda^2)}\right\}. \quad (20)$$

The quantity in the curly brackets in the last equality can become negative, which is shown in the bottom row of Fig. 7 by plotting the right-hand side (rhs) of the above equation (dashed lines). In the shown range of l^2, Eq. (20) is especially well satisfied for the parameters from Fit 2. For Fit 1 the equality is reached for much larger (not shown) values of $l^2=\mu^2$.

In Ref. [1] the critical line in the (x,Q^2) plane was defined which marks the transition to the saturation region where a new behavior of the structure function, $F_2\sim Q^2$, emerges. Near this line, the characteristic size of the $q\bar{q}$ di-

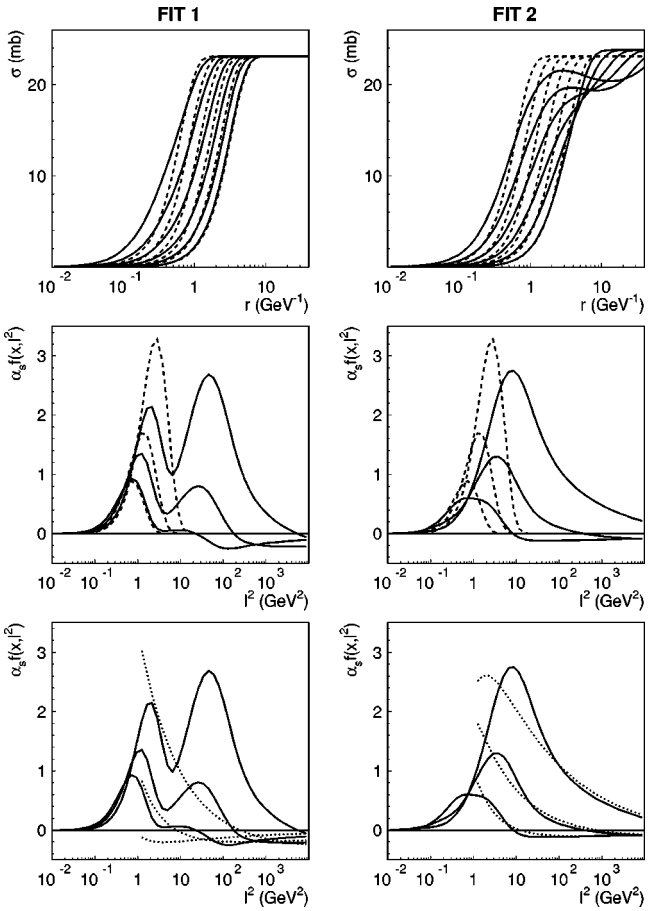

FIG. 7. The dipole cross section $\hat{\sigma}(x,r)$ (upper row) for $x=10^{-2}\ldots10^{-6}$ (from right to left) and the gluon amplitude $\alpha_s f(x,l^2)$ at $x=10^{-2}\ldots10^{-4}$ (from bottom to top) for the two fits. The solid lines correspond to the DGLAP improved model while the dashed lines describe the saturation model (2). The dotted lines in the bottow row show the rhs of Eq. (20).

pole, $\bar{r}\simeq 2/Q$, equals the saturation radius $R_0(x)$, see Sec. I. In this case the argument of the exponent in Eq. (2) equals one,

$$Q^2R_0^2(x)=1, \tag{21}$$

and $\hat{\sigma}(x,\bar{r})\sim\sigma_0$. We adopt the same criterion for the critical line in the DGLAP improved saturation model (8). Thus, we have the following condition:

$$\frac{4\pi^2}{3\sigma_0Q^2}\alpha_s(\mu^2)xg(x,\mu^2)=1, \tag{22}$$

where $\mu^2=CQ^2/4+\mu_0^2$. Equation (22) is an implicit equation for the critical line $Q^2=Q_s^2(x)$, shown in Fig. 8 for the two fits. As expected, for Fit 1 the found critical line is not different from that defined in the original saturation model (dashed line) and the transition region stays around 1 GeV^2 in the HERA kinematics (lower band). For Fit 2 the critical line is situated at lower values of Q^2 (around 0.5 GeV^2). It is interesting to note that both fits predict that in the THERA

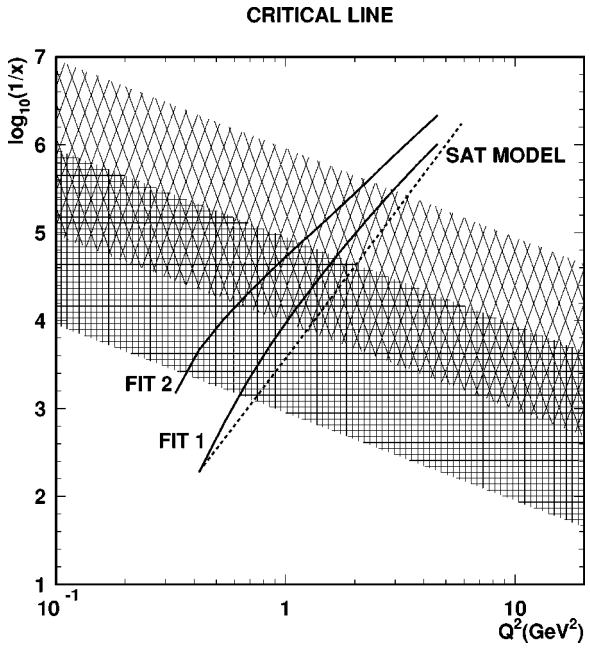

FIG. 8. The position of the critical line in the (x,Q^2) plane in the DGLAP improved model (solid lines) and the original saturation model (dashed line). The bands indicate acceptance regions for the colliders HERA (lower) and future THERA (upper).

kinematic range (upper band) the saturation region lies at $Q^2\approx 2$ GeV^2, which puts the perturbative QCD description of saturation effects on more solid ground.

IV. DIFFRACTION

One of the main advantages of dipole models is their straightforward description of diffractive processes. The generalized optical theorem applied in the framework of the dipole picture allows us to express the cross section for diffractive $q\bar{q}$ production in which proton remains intact as

$$\left.\frac{d\sigma_{dif}^{\gamma^*p}}{dt}\right|_{t=0}=\frac{1}{16\pi}\int d^2r\int dz\,\psi_{T,L}^*(Q,r,z)\hat{\sigma}^2(x,r)\times\psi_{T,L}(Q,r,z), \tag{23}$$

where $t=\Delta^2$, and Δ is the four-momentum transfered into the diffractive system from the proton. In addition to the contributions of the $q\bar{q}$ states it is important to include the contributions of the $q\bar{q}g$ final states [17].

In the phenomenological analysis [2], the $q\bar{q}g$ diffractive amplitude was computed in the two-gluon exchange approximation with an additional assumption of strong ordering of transverse momenta of the $q\bar{q}$ pair and the gluon. This allows us to treat the $q\bar{q}g$ system as a color octet dipole $(8\bar{8})$ in the transverse coordinate representation. Compared to the triplet dipole, the coupling of two t-channel gluons in the singlet state to the octet dipole carries the relative weight $C_A/C_F=2N_c^2/(N_c^2-1)$. Thus, in order to take into account

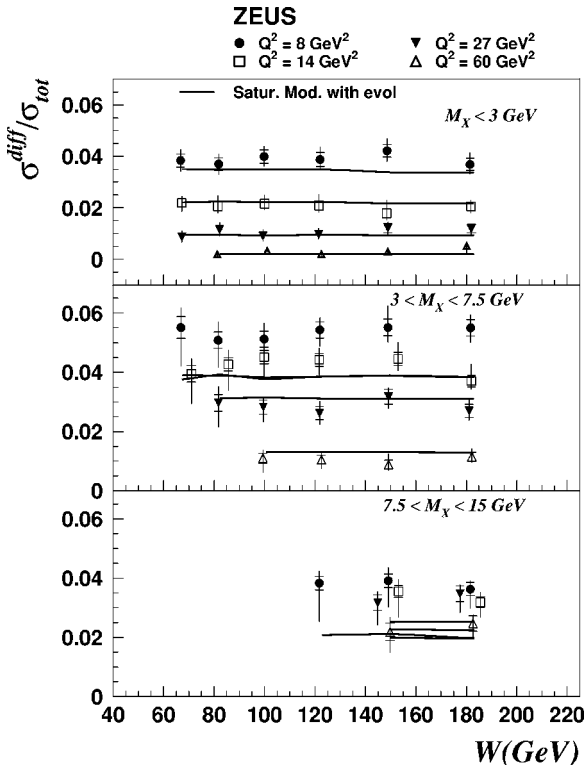

FIG. 9. The ratio of $\sigma_{diff}/\sigma_{tot}$ versus the $\gamma^* p$ energy W. The data are from ZEUS and the solid lines correspond to the results of the DGLAP improved model with massless quarks (Fit 2).

the repeated exchange of a two-gluon system, the equation (8) for the triplet dipole cross section is modified for the octet dipole as

$$\hat{\sigma}_{gg}(x,r)=\sigma_0\left\{1-\exp\left(-\frac{C_A}{C_F}\frac{\pi^2 r^2 \alpha_s(\mu^2) x g(x,\mu^2)}{3\sigma_0}\right)\right\}. \tag{24}$$

The above modification is done in the spirit of multiple Pomeron exchange, i.e. the term proportional to $(r^2)^n$, resulting from the expansion of the exponent in Eq. (24), would correspond to n exchanged Pomerons with an appropriate color factor $(C_A/C_F)^n$. In addition, compared to the diffractive $q\bar{q}$ production, the cross section formula for a diffractive $q\bar{q}g$ system contains an overal factor $(N_c^2-1)/N_c$.

One of the most important results of the original saturation model was that, at fixed Q^2, the ratio of the inclusive diffractive cross section and the total $\gamma^* p$ cross section is nearly constant in agreement with data. This prediction is not changed in the DGLAP improved saturation model since we modified only the short distance part of the dipole cross section. Even in the case of Fit 2, the constant ratio is preserved, as shown in Fig. 9, in contrast to the attempts in [4]. The theoretical curves in these figures are computed using the Fit 2 results, and the experimental data are taken from ZEUS [18]. The results for the Fit 1 computation differ only slightly from the Fit 2 conputation.

The diffractive data shown in Fig. 9 were obtained without the experimental identification of the forward going proton. Therefore, as described in [18], this data have a substantial contribution of the proton dissociation process which was estimated as $31\pm 15\%$. To take into account this contribution, the prediction of our model shown in Fig. 9 were multiplied by a normalization factor of $1/(1-0.31)=1.45$. The agreement of the height of the predicted cross section with the data is satifactory only within the relativly large error of the estimated proton dissociation factor.

We also made a comparison of our predictions with the recent preliminary diffractive data in which the forward going proton was identified in the ZEUS Leading Proton Spectrometer (LPS) [19]. Good agreement was found which gives further support to the dynamical picture of the $\gamma^* p$ interactions developed in this and previous papers on the saturation model.

V. CONCLUSIONS

In this paper we have proposed a modification of the saturation model which takes into account the QCD DGLAP evolution of the gluon distribution. Fitting the parameters of our model we found a solution that describes the new HERA data on F_2 significantly better than the original saturation model, especially in the region of larger Q^2. The agreement with the DIS diffractive HERA data is also kept.

Somewhat surprisingly, we found another set of parameters which lead to even better data description departing from the original saturation model. For this description, we set the effective quark mass of the original model equal to zero, and in our comparison with the HERA data we have disregarded photoproduction data points. We found indications that this solution represents a slightly different physical picture: the initial gluon density no longer rises at small x, and QCD-evolution plays a much more significant role than in our first solution. The fact that the effective quark mass of the original model has its strongest influence in the limit $Q^2\to 0$ suggests that the large-r behavior of the photon wave function requires further considerations.

We have found it useful to discuss the various versions of the saturation model not only in the r-space but also in momentum space since the latter provides more direct connection with exclusive final states. As a future step, it will be instructive to trace saturation effects in less inclusive cross sections.

We consider the modification of the saturation model presented in this paper as a first step of a more systematic program. The success of the original model indicates that this simple ansatz contains elements of the correct dynamics. Next, we have to analyze this model within QCD and to find the necessary corrections. With precise HERA data on various reactions becoming available [20], all modifications have to be testetd by careful comparisons.

ACKNOWLEDGMENTS

We thank Jan Kwiecinski and Misha Ryskin for useful discussions. This research has been supported in part by the Polish KBN grant No. 5 P03B 144 20 and the Deutsche Forschungsgemeinschaft.

[1] K. Golec-Biernat and M. Wüsthoff, Phys. Rev. D **59**, 014017 (1999).
[2] K. Golec-Biernat and M. Wüsthoff, Phys. Rev. D **60**, 114023 (1999).
[3] K. Golec-Biernat and M. Wüsthoff, Eur. Phys. J. C **20**, 313 (2001).
[4] E. Gotsman, E. Levin, M. Lublinsky, U. Maor, E. Naftali, and K. Tuchin, J. Phys. G **27**, 2297 (2001); E. Levin and M. Lublinsky, Phys. Lett. B **521**, 233 (2001).
[5] J.R. Forshaw, G. Kerley, and G. Shaw, Phys. Rev. D **60**, 074012 (1999); Nucl. Phys. **A675**, 80 (2000); E. Gotsman, E.M. Levin, U. Maor, and E. Naftali, Eur. Phys. J. C **10**, 689 (1999); M. McDermott, L. Frankfurt, V. Guzey, and M. Strikman, *ibid.* **16**, 641 (2000).
[6] L. Frankfurt, A. Radyushkin, and M. Strikman, Phys. Rev. D **55**, 98 (1997).
[7] A.D. Martin, R.G. Roberts, W.J. Stirling, and R.S. Thorne, Eur. Phys. J. C **23**, 73 (2002).
[8] S. Catani, M. Ciafaloni, and F. Hautmann, Phys. Lett. B **242**, 97 (1990); Nucl. Phys. **B366**, 657 (1991); J.C. Collins and R.K. Ellis, Nucl. Phys. **B360**, 3 (1991); E.M. Levin, M.G. Ryskin, Yu.M. Shabel'sky, and A. Shuvaev, Yad. Fiz. **53**, 1059 (1991) [Sov. J. Nucl. Phys. **53**, 657 (1991)].
[9] N.N. Nikolaev and B.G. Zakharov, Phys. Lett. B **332**, 184 (1994).
[10] A. Bialas, H. Navelet, and R. Peschanski, Nucl. Phys. **B603**, 218 (2001).
[11] ZEUS Collaboration, J. Breitweg *et al.*, Phys. Lett. B **487**, 53 (2000).
[12] ZEUS Collaboration, S. Chekanov *et al.*, DESY-01-064.
[13] H1 Collaboration, C. Adloff *et al.*, Eur. Phys. J. C **21**, 33 (2001).
[14] E665 Collaboration, M.R. Adams *et al.*, Phys. Rev. D **54**, 3006 (1996).
[15] ZEUS Collaboration, S. Chekanov *et al.*, Nucl. Phys. **B627**, 3 (2002).
[16] K. Golec-Biernat, J. Phys. G **28**, 1057 (2002).
[17] J. Bartels, J. Ellis, H. Kowalski, and M. Wüsthoff, Eur. Phys. J. C **7**, 443 (1999).
[18] M. Derrick *et al.*, Eur. Phys. J. C **6**, 43 (1999).
[19] ZEUS Collaboration, International Europhysics Conference, Budapest, 2001, Abstract 566.
[20] H1 Collaboration, C. Adloff *et al.*, Phys. Lett. B **520**, 183 (2001).